Molecular dynamics simulation of melting and structural evolution of transition bimetallic nanowires.

Subramanian K.R.S. Sankaranarayanan, Venkat R. Bhethanabotla[*] and Babu Joseph
Sensors Research Laboratory, Department of Chemical Engineering,
University of South Florida, Tampa, Florida, 33620, USA.

Abstract

Bimetallic nanowires find applications in catalysis and sensing. In sensing applications, the increased surface area and surface segregation of these nanowires results in superior selectivity, sensitivity and speed of response. Pd and Pd-alloy nanowires find use in hydrogen sensing. Understanding the thermal characteristics of these bimetallics is important to the design and synthesis of these nanowires.

The thermal characteristics of different bimetallic transition metal nanowires (Pd-Cu, Pd-Pt and Pd-Rh) with diameters ranging from 2.3 nm to 3.5 nm were studied using molecular dynamics utilizing the quantum Sutton-Chen potential function. Monte-Carlo simulations employing bond order simulation model were used to generate the initial configurations. The initial configurations consisted of surface segregated structures. The atoms with low surface energy segregated to the lower coordination sites, resulting in contrasting segregation profiles of Pd for the three nanowires. The melting temperatures were found by studying the variations in thermodynamic properties such as potential energy and heat capacity and structural properties such as bond orientational order parameter and Wigner values. Structural transformations associated with melting phenomenon were identified using bond orientational order parameter values. Analysis of density profiles along the nanowire cross-section and axis were used to identify the mechanism of melting in nanowires.

I. Introduction

Metal nanowires have attracted much attention in recent years primarily due to their importance in fundamental low dimensional physics and their potential applications in nanoscale materials and devices[23]. These nanowires exhibit physical, chemical and electronic properties which are different from both bulk materials as well as single molecules[9,11, 27]. The unique properties of nanowires help them find applications in a variety of different areas such as sensing, catalysis, drug delivery, semiconductors, microelectronics etc. With the miniaturization of devices, it has become important to understand the structure and properties of these nanowires. One such nanostructure is Pd and its alloys which find extensive use in hydrogen sensing and catalysis. The key to potential applications of nanowires lies in their small size and structure. This makes knowledge and control over their size and shape distributions, surface compositions as well as crystal structure, critical to improved designs of the same.

Considerable experimental and theoretical research has been dedicated to understanding the thermodynamics and kinetics of nanowire growth and stabilization[11,15,17,41,7,28,36]. Nanowires are not observed spontaneously in nature and require to be produced in laboratory. Recent experimental studies have revealed the formation of stable ultra thin nanowires of gold having a length to diameter ratios of over ten [37,38]. Nanowires of Ag-Pt with lengths up to 3.5 μm and

diameters between 3 and 20 nm have been produced by irradiation of aqueous solutions of Ag-Pt ions with gamma rays[10]. Other methods to produce bimetallic nanowires with high aspect ratios are also gaining interest [40]. One of the challenging issues is the control over the size and morphology of these nanostructures. The melting properties of these metallic nanowires and their associated effect on the size, shape, and composition would have a bearing on the method of synthesis, processing, and the performance of these nanowires in their various areas of applications. Experimental investigations have revealed the growth of InAs to be limited by the melting temperature of Au-In alloy.

The melting points of nanowires decrease with decreasing sizes and their values are much below the bulk melting points[17,18,20,46,41,43]. The large ratio of surface to bulk atoms is primarily responsible for this lowering effect. Experimentally, it is difficult to observe the microscopic processes associated with melting. Computer simulations offer an effective tool to study the properties of nanowires and complement the experimental efforts.

A molecular dynamics study of the melting of one dimensional zirconium wire indicated melting of nanowires to initiate from the inner core shell atoms[19]. The diffusion of the central atoms in Palladium nanowires was found to result in the beginning of melting. The melting of gold nanowires indicated surface melting temperature be representative the overall wire melting temperature[44]. This behavior is very much different from those of nanoclusters where the onset of melting results from enhanced movement of the less restrained surface atoms[8]. A coexistence of liquid and solid phases was also observed in the melting process of titanium nanowires [18]. Similarly, a study of ultra thin titanium nanowires with diameters less than 1.2 nm, indicate no clear characteristic first order transition during the melting process[42]. Structural transformations from a helical multiwalled to a bulk like rectangular structure have also been observed for 1.7 nm titanium wires.

Bimetallic nanomaterials have been found to be better suited for catalytic and sensing applications than their monometallic counter parts [34]. However, much less attention has been devoted to the study of these bimetallics because of complex phenomena such as surface segregation and micro-mixing occurring in finite sized structures such as nanowires. For a given composition of the bimetallics, the microstructure is dictated by surface energies and mixing energies of the constituent atoms [47,48,49]. Atoms with lower surface energies tend to segregate to low coordination number sites, the extent of which is determined by the interplay between surface energies, mixing energies and entropy. There is enough experimental evidence to indicate the occurrence of this phenomenon in nanowires of Pd-Ag and Pt-Ag [22].

Although there have been extensive theoretical investigations into the melting characteristics of nanowires, fewer efforts have focused on the study of bimetallic nanowires. In the present work, we study thermal characteristics of one dimensional Pd alloy nanowires of different sizes and compositions using molecular dynamics (MD) simulations employing quantum Sutton-Chen potential function. Alternate starting configurations have been employed to study the effect of the nature of closed packing on the thermal stability of nanowires.

II. Initial configuration set-up

All the transition elements have an fcc structure in bulk form. Hence, a large block of fcc was formed from an fcc unit cell by replicating in ABC direction and cylindrical structures representing nanowires of varying diameters ranging from 2.3 nm to 3.5 nm were created using different cutoff radii. The length to diameter ratio was varied to ensure that the results are not influenced by the periodic boundary conditions. Alternate starting configurations comprising of hcp nanowires were also generated using hcp fractional coordinates.

In order to identify the atomic distribution of the constituent atoms for a given composition of the bimetallic, these structures were subjected to a Metropolis Monte-Carlo simulation employing a bond order simulation (BOS) model [47], to generate the minimum energy initial configuration which was subsequently used for studying the melting phenomena. The BOS model was modified to include periodic boundary condition along the nanowire axis.

The stable configurations consisted of surface segregated structures with lower surface energy atoms preferentially located at the surface. The extent of segregation depends on the factors such as surface energy, mixing energy and entropy. The final microstructure depends on the interplay amongst these factors. Therefore, Cu in Pd-Cu, and Pd in Pd-Pt and Pd-Rh nanowires occupied most of the surface sites. These structures were utilized as starting points for studying the thermal characteristics of bimetallic nanowires.

III. Computational details

Molecular dynamics simulations using DLPOLY were used to gain insights into the melting process at the atomistic level. The thermodynamic and transport properties were derived as time averages over particle positions and velocities. The quantum Sutton-Chen (QSC) potential function[29,30,31,11] was employed to model metal-metal interactions. The potential parameters used in the simulations are listed in Table 1.

Table 1. Potential parameters used in MD simulations for metal-metal interactions.

Quantum Sutton-Chen	n	m	ε (eV)	c	a(Å)
Pd	12	6	3.2864e-3	148.205	3.8813
Pt	11	7	9.7894e-3	71.336	3.9163
Rh	13	5	2.4612e-3	305.499	3.7981
Cu	10	5	5.7921e-3	84.843	3.603

The MD simulations were carried out in an ensemble approximating the canonical with a constant number of atoms N and volume V with periodic boundary condition applied along the nanowire axis. A constant temperature Berendson thermostat[2] with a relaxation time of 0.4 ps was used. The equations of motion were integrated using Verlet leapfrog algorithm[1,12] with time step of 0.001 ps. The nanowires were initially subjected to mild annealing in the 0-300 K interval which was followed by heating to 1800 K in increments of 100 K. Near the melting point, the temperature increments were reduced to 10 K to account for the large temperature

fluctuations. The simulations were carried out for 400 ps of equilibration followed by 200 ps of production time for generating time averaged properties.

IV. Results and discussion

The following subsections discuss identification of the melting point as well as characterization of the structural changes associated with the phase transition for the three bimetallics at 50% Pd representative composition. Particular emphasis is on Pd-Cu and Pd-Rh nanowires due to the contrasting segregation patterns of Pd observed in the two bimetallic. Dynamic properties calculated at different temperatures leading up to the phase transition and beyond are used to gain insights into the mechanism of nanowire melting. Phase diagrams representing composition dependency of melting point for the three alloy nanowires are generated and compared to same sized nanoclusters as well as bulk alloys.

i. Melting point identification

The transition temperature from solid to liquid phase is identified by studying variations in thermodynamic properties such as potential energy and specific heat capacity as well as structural properties such as bond order parameter and Wigner values. The details are discussed below:

a) Thermodynamic properties

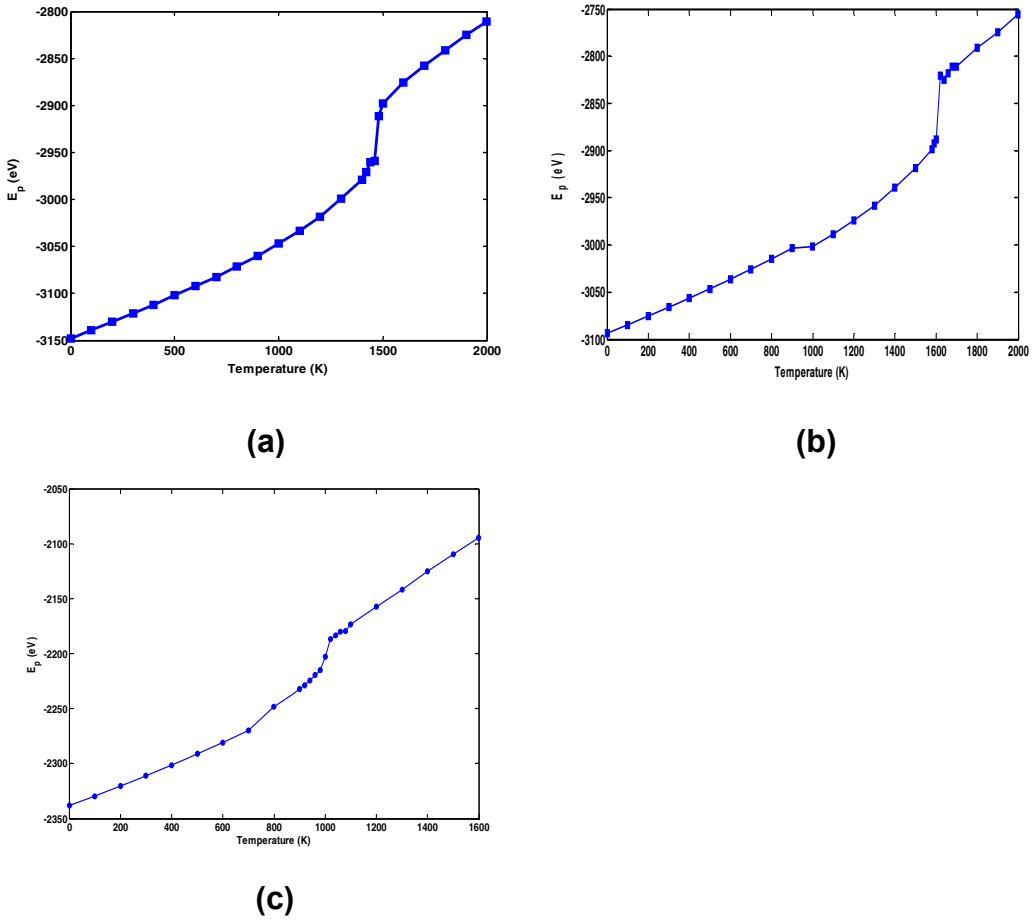

Figure 1. Variation of potential energy with temperature for (a) Pd-Pt (b) Pd-Rh and (c) Pd-Cu.

Figure 1 (a), (b) and (c) show the temperature dependence of potential energy for $(Pd_{0.5}\text{-}Pt_{0.5})_{2.34nm}$, $(Pd_{0.5}\text{-}Rh_{0.5})_{2.31nm}$, and $(Pd_{0.5}\text{-}Cu_{0.5})_{2.26nm}$ nanowires. The phase transition from solid to liquid phase can be identified by simple jump in the total potential energy curve. This corresponds to a melting temperature of 1470 ± 10 K, 1610 ± 10 K, and 1010 ± 20 K for $(Pd_{0.5}\text{-}Pt_{0.5})_{2.34nm}$, $(Pd_{0.5}\text{-}Rh_{0.5})_{2.31nm}$, and $(Pd_{0.5}\text{-}Cu_{0.5})_{2.26nm}$ nanowires, respectively. Pd-Cu nanowire shows a more continuous transformation in comparison to Pd-Pt and Pd-Rh nanowires. This feature could be attributed to increased surface melting of Cu atoms in Pd-Cu nanowires than Pd atoms for Pd-Rh and Pd-Pt nanowires. The melting point increases with size for the three bimetallics. The composition dependency of the nanowire melting point is discussed in the subsequent sections.

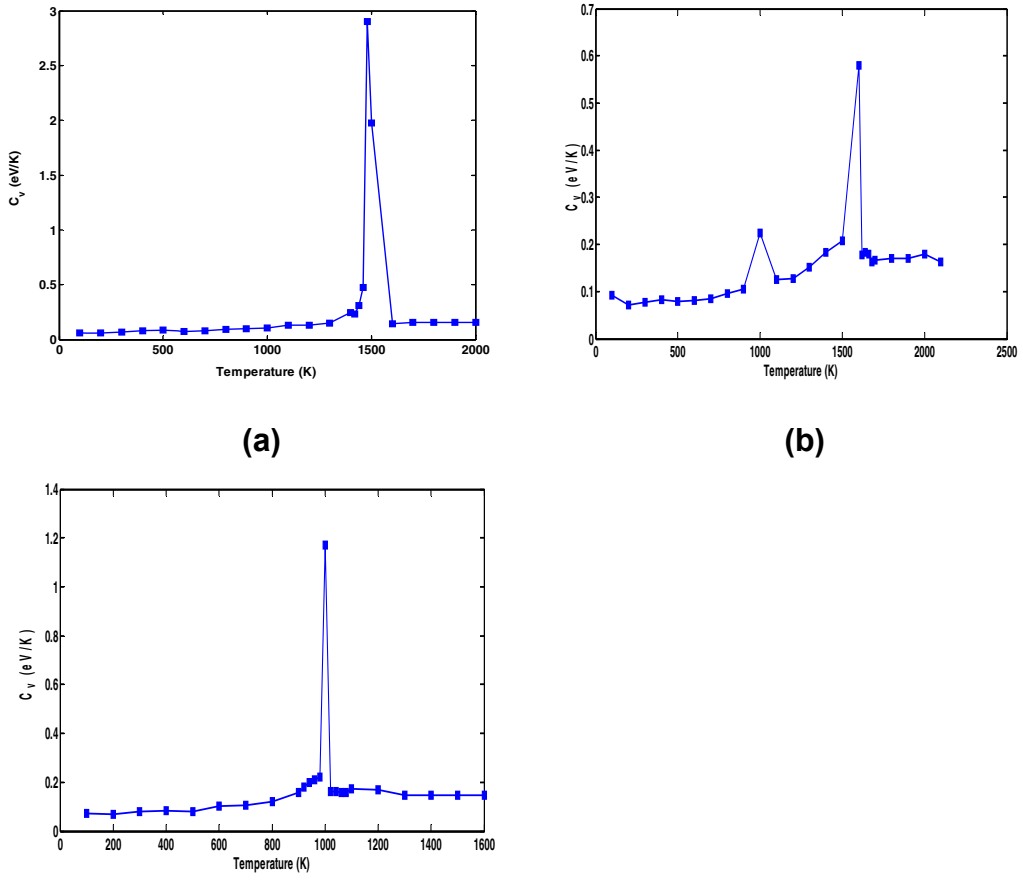

Figure 2. Variation of specific heat capacity with temperature for (a) Pd-Pt (b) Pd-Rh and (c) Pd-Cu.

The specific heat capacity (C_v) in a weak coupling ensemble such as that achieved with the Berendson thermostat can be written as a function of fluctuations in the potential energy $\langle(\delta Ep)^2\rangle$[12]**Error! Reference source not found.**. Strictly speaking, the specific heat capacity also includes

the contribution arising from the ideal gas kinetic energy, which is however constant and hence has no effect on the change of C_v with temperature.

$$C_v = \frac{k < (\delta E_p)^2 >}{(kT)^2 - 2\alpha < (\delta E_p)^2 > /3N} \tag{4.1}$$

where $< (\delta E_p)^2 >=< E_p^2 > - < E_p >^2$ and α is the ratio of the standard deviations of kinetic and potential energies.

$$\alpha = \sqrt{< (\delta KE)^2 > / < (\delta Ep)^2 >} \tag{4.2}$$

Morishita has proved that a weak coupling ensemble approaches a canonical ensemble for very short relaxation times (α ≈ 0) and to a microcanonical ensemble for longer relaxation times (α ≈ 1). In the present case, the Berendson thermostat with a coupling parameter of 0.4 ps leads to α ≈10^{-4}, making the calculation for specific heat capacity similar to that of a canonical ensemble as given in equation (4.3)

$$C_v = \frac{k\left\langle (\delta E_p)^2 \right\rangle}{(kT)^2} \tag{4.3}$$

The constant volume specific heat capacity (C_v) at different temperatures is shown in Fig. 2 for the three bimetallic nanowires having 50% Pd composition. The phase transition from solid to liquid is identified by the maximum in the C_v curve. This corresponds to 1470 ± 10 K, 1610 ± 10 K, and 1010 ± 20 K for $(Pd_{0.5}\text{-}Pt_{0.5})_{2.34nm}$, $(Pd_{0.5}\text{-}Rh_{0.5})_{2.31nm}$, and $(Pd_{0.5}\text{-}Cu_{0.5})_{2.26nm}$ nanowires, respectively. In addition, a sharp peak is observed at 1000 K for $(Pd_{0.5}\text{-}Rh_{0.5})_{2.31nm}$ nanowire which is 600 K below the melting point for the same. This could be attributed to isomerization or structural changes in the nanowire. A similar characteristic occurs for Pd-Pt nanowires in a different composition range (15-40% Pd). Our findings indicate that all the three nanowires undergo structural transformation on heating with wide differences in the solid-solid and solid-liquid phase transformation observed in a particular bimetallic composition range for a given nanowire size. Thus, the onset of solid-solid transformation occurs at different temperatures for a given Pd composition in the three bimetallics and is dictated by the relative strengths of the metal-metal interactions. Better insights into the nature of solid-solid transformation could be obtained by utilizing bond orientational order parameters.

b) Structural properties

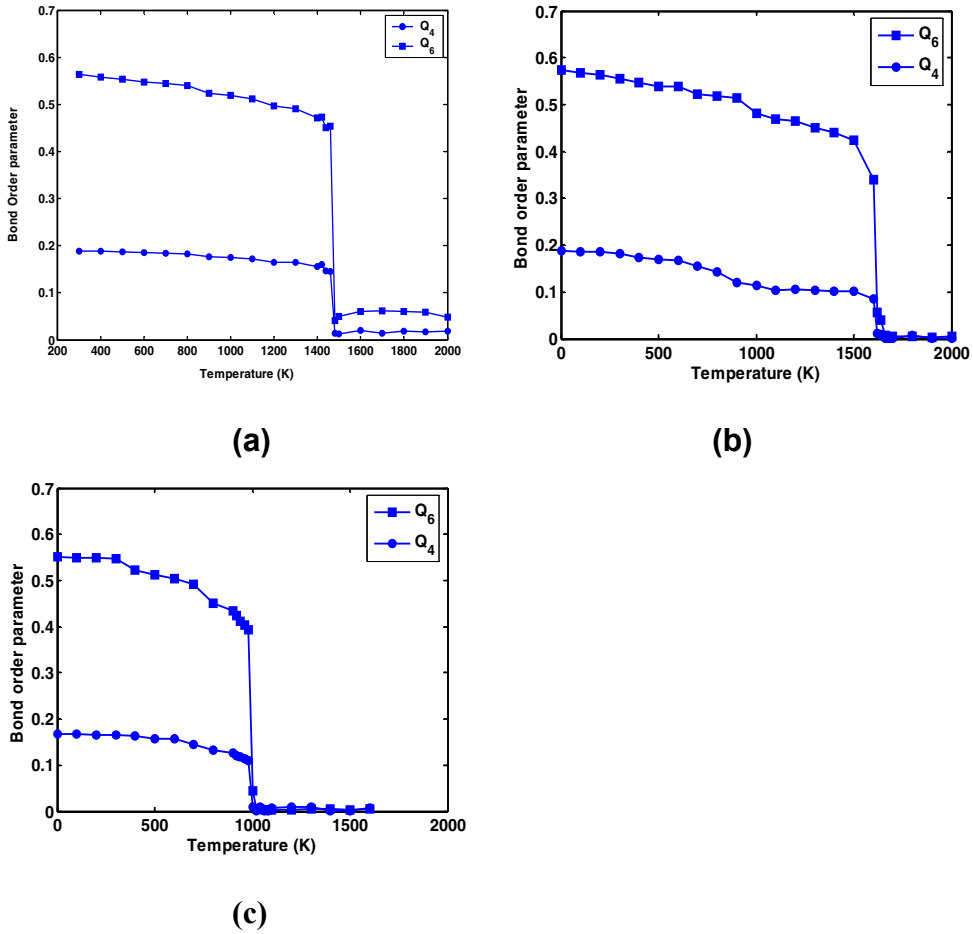

Figure 3. Variation of bond orientational order parameters with temperature for (a) Pd-Pt (b) Pd-Rh and (c) Pd-Cu.

One of the several criteria's used to identify local and extended orientational symmetries is the bond orientational order parameter method35. Analysis of the wire structure as well as distinction between atoms in solid (closed packed) and liquid environment generated during the melting process could be identified by using different signatures of the orientational order parameters. The value of the global bond orientational order parameter Q_l (Table 2) in a solid structure depends on the relative bond orientations and has a unique value for each crystal structure.

The atoms in a solid undergo vibrations about their equilibrium positions leading to distortion of the crystal structure which is characterized by Q_4 and Q_6 values. The magnitude of the nonzero $\{Q_l\}$ values depends on the definition of nearest neighbors and can be changed by including surface bonds in the average. The cutoff distance (r_{cut}) for identifying the nearest neighbors was taken to be 3.6 A at 300 K. This corresponds to the position of the first minimum in the pair correlation function for fcc Pd-Pt. The cut-off distance (rcut) at other temperatures and different wires were similarly identified.

Table 2. Bond orientational order parameter values for various geometries.

Geometry	Q_4	Q_6
fcc	0.19094	0.57452
hcp	0.09722	0.48476
bcc	0.03637	0.51069
icosahedral	0	0.66332
sc	0.76376	0.35355
liquid	0	0

The temperature dependence of the bond orientational order parameters (Q_4 and Q_6) is shown in Fig. 3 for the three bimetallics. Comparison of the Q_4 and Q_6 order parameters in Fig. 3 with those given in Table 3 indicate structural transformation to occur in all the three bimetallic nanowires. A solid-solid transformation from fcc to hcp occurs at 800 K for Pd-Cu, 1300 K for Pd-Pt and 1000 K for Pd-Rh nanowires. Comparisons with the melting points for the same indicate an early onset in case of Pd-Rh than Pd-Cu and Pd-Pt.

The change in order parameters of Pd-Cu is much more continuous than in the case of Pd-Rh and Pd-Pt nanowires which could be attributed to an early onset and greater extent of surface melting. Fig. 3 (a) and (b) indicate Pd-Rh to surface melt more in comparison to Pd-Pt. These observations are in line with the experimental studies which suggest a surface melting order of Cu>Rh>Pt. At the melting point, all the order parameters show a sudden decrease to zero indicative of the phase transformation to liquid. These agree well with the melting points calculated using potential energy and specific heat capacity curves.

ii.Mechanism of melting in nanowires

Insights into the nanowire melting mechanism could be obtained by analysis of density profiles along the nanowire axis and cross-section as well as shell based diffusion coefficients and velocity auto-correlation functions.

a) Density profiles

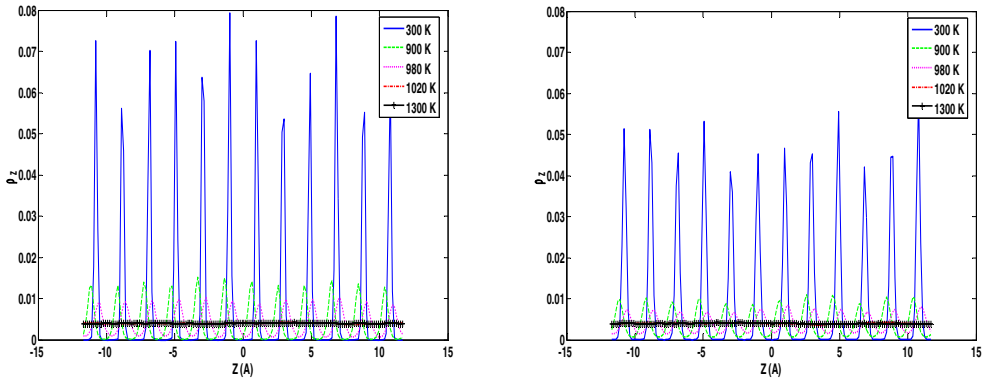

Figure 4. Atomic distribution profiles along Pd-Cu nanowire axis for (a) Pd (b) Cu.

Figure 4 (a) and (b) show the atomic distribution of Pd and Cu atoms along the axial direction, during the melting of $(Pd_{0.5}\text{-}Cu_{0.5})_{2.26nm}$ nanowire. At lower temperatures, solid like features are preserved as indicated by the distinct peaks in the axial density profile. With an increase in temperature, the peaks become broader, suggestive of a relatively larger movement of metal atoms. The peaks remain distinct in the 300-900 K range for both Cu and Pd atoms in $(Pd_{0.5}\text{-}Cu_{0.5})_{2.26nm}$ nanowire. The small shift in the peak at 900 K suggests a much smaller movement of the metal atoms in the axial direction (<0.5 Å).

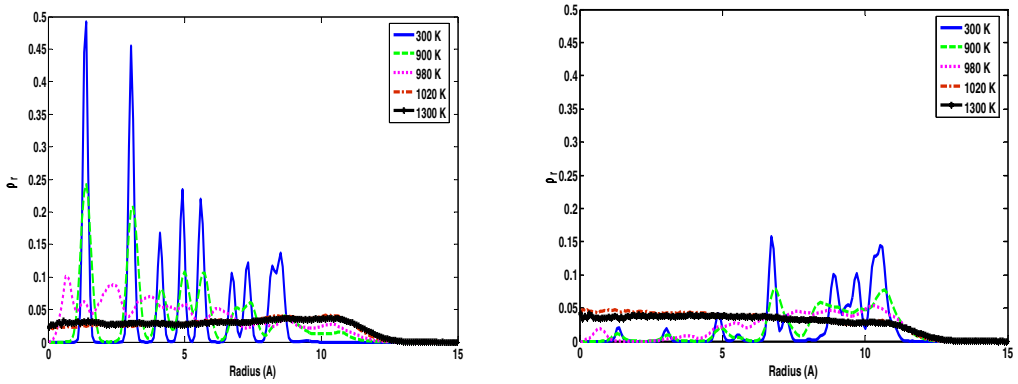

Figure 5. Atomic distribution profiles along Pd-Cu nanowire cross-section for (a) Pd (b) Cu.

On the other hand, the lowering and merging of peaks at 900 K in the radial density profile (Fig. 5(a) and (b)) for both Cu and Pd atoms (especially for radius > 5 Å) indicates much larger movement of atoms along the nanowire radius. The wire diameter increases as a result of such movement. Also, the peaks located in the outer region merge first followed by those located on the inside indicating surface melting of nanowire. At the melting point, the distribution becomes smooth indicative of transformation to liquid phase.

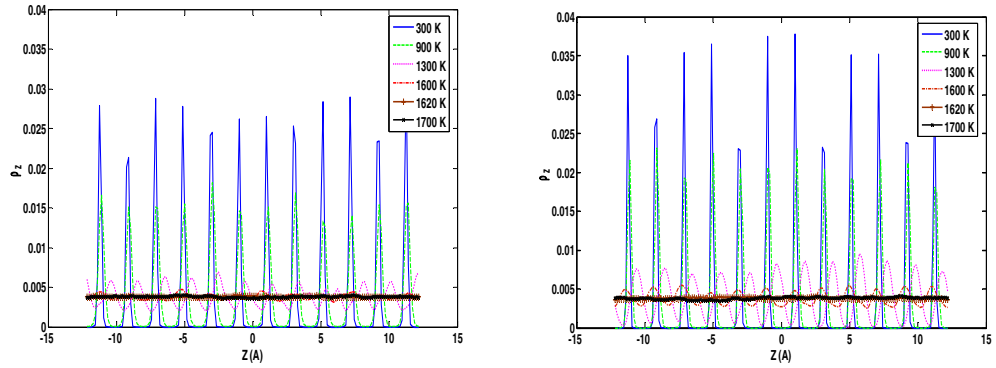

(a) **(b)**

Figure 6. Atomic distribution profiles along Pd-Rh nanowire axis for (a) Pd (b) Rh.

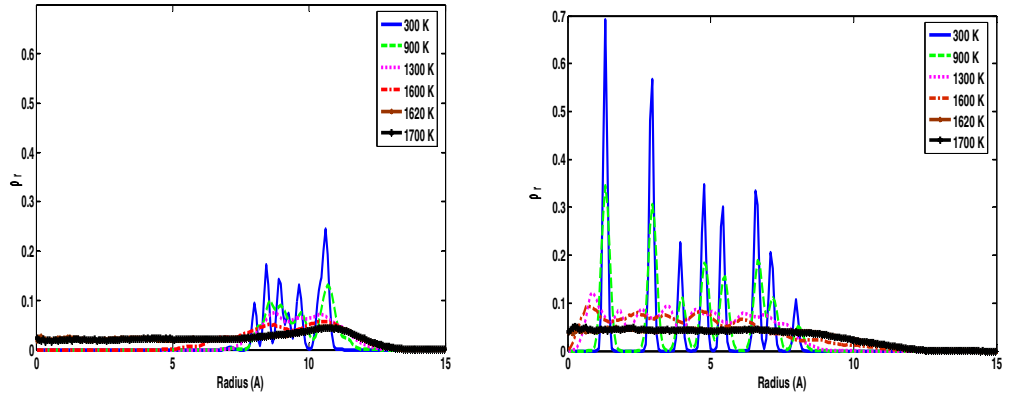

Figure 7. Atomic distribution profiles along Pd-Rh nanowire cross-section for (a) Pd (b) Rh.

Similar surface melting characteristics are also observed for Pd-Rh (Fig. 6 and 7) and Pd-Pt nanowires. A relatively larger axial movement as suggested by the shift in the peaks is observed in case of Pd-Rh than Pd-Cu and Pd-Pt nanowires. At temperatures close to the melting point, the axial movement also becomes significant.

V. Conclusion

The thermal characteristics of bimetallic nanowires (Pd-Cu, Pd-Rh and Pd-Pt) have been investigated in the present study. The melting behavior is characterized by pre-melting of surface segregated atoms (Cu in case of Pd-Cu and Pd in Pd-Pt and Pd-Rh) followed by homogeneous melting of core atoms (Pd in Pd-Cu Rh in Pd-Rh and Pt in Pd-Pt). The melting point is identified by studying temperature variations of thermodynamic properties such as potential energy and specific heat capacity as well as structural property such as bond orientational order parameter and suggests an order of Pd-Cu>Pd-Rh>Pd-Pt for the onset of surface melting. Although the melting point of nanowires is higher than nanoclusters of similar size and composition, they are much lower than bulk. The bond orientational order parameters suggest a solid-solid transformation to occur for all the three nanowires. An early onset of such a transformation occurs at different composition ranges of Pd in the three alloy nanowires for a given size depending on the relative strength of the metal-metal interaction. Density profiles calculated along the axial and radial direction of the nanowires suggest larger atomic movement in the radial direction than axial for all the three bimetallics. Thus, melting in nanowires is initiated by higher radial movement and proceeds from the surface to the core. This two dimensional melting mechanism differs from that observed for similar nanocluster[12] size and composition.

References:

* Corresponding author email: Venkat@eng.usf.edu

1. Allen, M.P and Tildesley, D.J. Computer Simulation of Liquids, (1987), Oxford University Press.
2. Berendson, H. J. C.; Postma, J. P. M.; Van Gunsteren, W. F.; DiNola, A.; Haak, J. R. J. Chem. Phys. (1984), 81(8), 3684-3690.
3. Biedermann, O. G.; Hebenstreit, W.; Shmid, M.; Redinger, J.; Podloucky, R. and Varga, P. Phys. Rev. Lett. (1996) 76, 4179.
4. Binasch, G.; Grunberg, P.; Saurenbach, F. and Zinn. W. Phys. Rev. B (1989) 39, 4828.
5. Burgi, L.; Jeandupeux, O; Hirstein, A.; Brune, H. and Kern, K. Phys. Rev. Lett. (1998) 81, 5370.
6. Cagin, T.; Kimura, Y.; Qi, Y.; Li, H.; Ikeda, H.; Johnson, W.L.; Goddard, W.A. III. Mater. Res. Soc. Symp. Proc. (1999), 554 (Bulk Metallic Glasses), 43-48.
7. Cheng, S-W. and Cheung, H-F. Appl. Phys. Lett. (2004), 85(23), 5709-5711.
8. Cleveland, C.L.; Luedtke, W.D.; Landman, U. Phys. Rev. Lett. (1998), 81(10), 2036-2039.
9. Crommie, M. F.; Lutz, C. P. and Eigler, D. M. Nature (1993)363, 524.
10. Doudna, C. M.; Bertino, M. F.; Blum, F. D.; Tokuhiro, A. T.; Lahiri-Dey, D.; Chattopadhyay, S.; Terry, J. J. Phys. Chem. B (2003), 107(13), 2966-2970.
11. Englander, O.; Christensen, D.; Kim, J.; Lin, L.; Morris, S. J. S. Nano Lett. (2005), 5(4), 705-8.
12. Haile, J. M., Molecular Dynamics Simulations: Elementary Methods. (1992) John Wiley and Sons. New York.
13. Hasegewa, Y. and Avouris, P. Phys. Rev. Lett. (1993) 71, 1071.
14. Himpsel, F. J. and Ortega, J. E. Phys. Rev. B (1994) 50, 4992.
15. Hochbaum, A. I.; Fan, R.; He, R.; Yang, P. Nano Lett. (2005), 5(3), 457-460.
16. Huh, S. H.; Nakajima, A. Appl. Phys. Lett. (2004), 85(25), 6149-6151.
17. Hui, L.; Pederiva, F.; Wang, B. L.; Wang, J. L.; Wang, G. H. Appl. Phys. Lett. (2005), 86(1), 011913/1-011913/3.
18. Hui, L.; Wang, B. L.; Wang, J. L.; Wang, G. H. Chemical Phys. Lett. (2004), 399(1-3), 20-25.
19. Hui, L.; Wang, B. L.; Wang, J. L.; Wang, G. H. J. Chem. Phys. (2004), 120(7), 3431-3438.
20. Hui, L.; Wang, B. L.; Wang, J. L.; Wang, G. H. J. of Chemical Phys. (2004), 121(18), 8990-8996.
21. Hwang, H-J. and Kang, J. W. Surf. Sci. (2003), 532-535 , 536-543.
22. Lahiri, D.; Bunker, B.; Mishra, B.; Zhang, Z.; Meisel, D.; Doudna, C. M.; Bertino, M. F.; Blum, F. D.; Tokuhiro, A. T.; Chattopadhyay, S.; Shibata, T. and Terry, Jeff. J. Appl. Phys. (2005), 97(9), 094304/1-094304/8.
23. Landman, U.; Luedtke, W. D.; Burnham N. A. and Colton, R. J. Science (1990) 248, 454.

24. Li, J.; Schneider, W. D. and Bemdt, R. Phys. Rev. B (1997) 56, 7656.
25. Morishita, T. J. Chem. Phys. (2000), 113(8), 2976-2982.
26. Nguyen, P.; Ng, H. T.; Kong, J.; Cassell, A. M.; Quinn, R.; Li, J.; Han, J.; McNeil, M. and Meyyappan, M. Nano Lett. (2003), 3(7), 925-928.
27. Parkin, S. S. P.; More, N. and Roche, K. P. Phys. Rev. Lett. (1990) 64, 2304.
28. Qi, W. H.; Wang, M. P.; Zhou, M. and Hu, W. Y. J. of Phys. D: Appl. Phys. (2005), 38(9), 1429-1436.
29. Qi, Y.; Cagin, T.; Johnson, W.L.; Goddard, W.A. III. J. Chem. Phys. (2001), 115(1), 385-394.
30. Qi, Y.; Cagin, T.; Kimura, Y.; Goddard, W.A. III. Phys. Rev. B (1999), 59(5), 3527-3533.
31. Qi, Y.; Cagin, T.; Kimura, Y.; Goddard, W.A. J. Comput. Aided Mater. Des. (2002), 8(2-3), 233-244.
32. Sankaranarayanan, S. K. R. S.; Bhethanabotla, V. R.; Joseph, B. Phys. Rev. B. (2005), 71(19), 195415/1-195415/15.
33. Schmidt, V; Senz Stephan and Gosele, U. Nano Lett. (2005 May), 5(5), 931-5.
34. Sinfelt, J. H. (1983), John Wiley & Sons, New York.
35. Steinhardt, P.J.; Nelson, D.R.; Ronchetti, M. Phys. Rev. B (1983), 28(2), 784-805.
36. Tan, T. Y.; Li, N.; Gosele, U. Appl. Phys. Lett. (2003), 83(6), 1199-1201.
37. Tokushi, K. Phys. Rev. B 63 (2001) 033309.
38. Tokushi, K. Phys. Rev. Lett. 81 (1998) 4448
39. Van Wees, B. J. ; van Houten, H.; Beenakker, C. W. J. ; Williamson, J. G. ; Kouvenhoven, L. P. ; van der Marel, D. and Foxon, C. T.. Phys. Rev. Lett. (1988) 60, 848.
40. Walter, E. C.; Murray, B. J.; Favier, F.; Penner, R. M. Adv. Mat. (Weinheim, Germany) (2003), 15(5), 396-399.
41. Wang, B.; Wang, G.; Chen, X.; Zhao, J. Phys. Rev. B. (2003) 67(19), 193403/1-193403/4.
42. Wang, B.; Wang, G.; Chen, X.; Zhao, J. Phys. Rev. B. (2003), 67(19), 193403/1-193403/4.
43. Wang, C-X; Wang, B; Yang, Y-H; Yang, G-W. J. Phys. Chem. B (2005), 109(20), 9966-9969.
44. Wang, J.; Chen, X.; Wang, G.; Wang, B.; Lu, W.; Zhao, J. Phys. Rev. B (2002), 66(8), 085408/1-085408/5.
45. Wen, Y-H; Zhu, Z-Z.; Zhu, R. and Shao, G-F. Physica E. (2004), 25(1), 47-54.
46. Wen, Yu-Hua; Zhu, Zi-Zhong; Zhu, Ruzeng; Shao, Gui-Fang. Physica E. (2004), 25(1), 47-54.
47. Zhu, L. and DePristo, A.E. J. Catalysis (1997), 167(2), 400-407.
48. Zhu, L. and DePristo, A.E. J. Chem. Phys. (1995), 102(13), 5342-5349.
49. Zhu, L.; Wang, R.; King, T.S.; DePristo, A.E. J. Catalysis (1997), 167(2), 408-411.